scientific reports

Check for updates

OPEN

Assessing antitumor effects of plasma-activated phosphate buffered saline in breast cancer cell 2D and 3D models

Darina Kužmová[1], Helena Gbelcová[2] & Zdenko Machala[1]✉

Cold plasma-based therapy shows potential as a new method of tumor reduction, especially beneficial for patients who do not respond positively to conventional therapy or struggle with health complications associated with such treatment. This study investigates the plasma-activated phosphate-buffered saline (PAPBS) that exhibits significant antitumor efficacy against human breast adenocarcinoma cells in a dose-dependent manner. The activation of phosphate-buffered saline (PBS) was performed using a cold atmospheric plasma of streamer corona discharge. By testing PAPBS on both paclitaxel-sensitive MCF-7 human breast adenocarcinoma cell line and its paclitaxel-resistant subline, MCF-7/PAX, it is shown that PAPBS significantly reduced cell viability and triggered apoptosis in both cell lines after a 1-h incubation. PAPBS effectively inhibited the growth of breast cancer cell 3D physiologically relevant tumor models—spheroids and caused their shrinkage depending on plasma treatment time and the duration of PAPBS exposure. Furthermore, cells in 3D models of resistant breast tumor cells completely lost their viability after 24-h treatment with PAPBS treated 30 min by plasma. These findings indicate that PAPBS enriched by RONS can overcome acquired drug resistance in breast cancer, representing a promising anticancer therapeutic strategy.

Keywords Cold plasma, Plasma-activated liquid, Antitumor effect, Breast cancer, Chemotherapy resistance, Spheroids

Despite decades of intensive research and development of anticancer therapies, cancer remains the second leading cause of death worldwide. For women, breast cancer is the most frequently diagnosed malignancy and one of the leading causes of cancer-related mortality, surpassing both lung and colorectal cancers. This reality highlights the urgent need for innovative therapeutic strategies against breast cancer. Approaches that can enhance existing treatments aim for curative outcomes while minimizing adverse effects, and in palliative care, improve patients' quality of life [1]. Although chemotherapy is a key strategy for breast cancer treatment, whether it is used as a neoadjuvant, adjuvant, or primary therapy, it faces challenges when breast cancer tumors exhibit drug resistance. This lack of a tumor response can be intrinsic or acquired, where initially sensitive tumors develop resistance during treatment [2].

Plasma medicine represents a potential innovative strategy in the fight against cancer. Cold atmospheric plasma (CAP) generates a reactive environment with extensive potential across a broad range of biomedical applications, from the sterilization of medical instruments to direct interactions with cells and tissues, the treatment of various skin diseases and the enhancement of wound healing [3]. However, there is a growing emphasis on studies demonstrating its antitumor effect and potential in cancer treatment.

The antitumor effect of CAP is mainly attributed to the reactive oxygen and nitrogen species (RONS) generated in the plasma due to the physical–chemical processes of the interaction of the plasma and ambient air. These species include hydroxyl radicals ·OH, hydrogen peroxide H_2O_2, nitrogen oxides N_2O, NO, NO_2, ozone O_3, and superoxide $O_2\cdot^-$[4].

RONS are involved in numerous physiological processes, including cell signaling, the immune response, and homeostasis [5]. They also function as important signaling molecules that regulate various aspects of cancer, including cell proliferation, survival, angiogenesis, and metastasis.

[1]Faculty of Mathematics, Physics and Informatics, Comenius University, 842 48 Mlynská Dolina, Bratislava, Slovakia. [2]Faculty of Medicine, Comenius University, Špitálska 24, 813 72 Bratislava, Slovakia. ✉email: zdenko.machala@fmph.uniba.sk

While low levels of RONS can stimulate cell proliferation, higher doses of RONS can cause DNA damage [6]. RONS penetrate the cell membrane while increasing their intracellular concentration and triggering oxidative stress. They react with amino acids and oxidize lipids in lipid bilayers, leading to cellular membrane and organelle damage [7]. Cellular damage then initiates specific cascades, ultimately leading to the activation of apoptotic mechanisms [8]. The induction of RONS-related stress is a widely utilized mechanism in anticancer therapies [9].

Cancer cells appear to be more vulnerable to the effects of RONS compared to normal cells, based on many studies [10–13]. This phenomenon can be explained by the higher RONS-related stress tolerance threshold in normal cells. Cancer cells already have elevated basal levels of ROS in part due to their oncogenic stimulation, increased metabolic activity, and mitochondrial malfunction. Plasma-generated exogenous RONS can therefore more easily exceed the tolerance threshold in cancer cells than in normal cells, creating a therapeutic dose window [14–17].

Another theory to explain the selective antitumor effect of plasma is based on the overexpression of aquaporins in many types of cancer cells, including breast cancer, glioma, hemangioblastoma, lung adenocarcinoma, laryngeal, colorectal, and ovarian cancer [18,19]. These transmembrane channels allow the transport of RONS across the membrane [20]. Additional cancer cells contain a reduced level of cholesterol in their cell membranes, making the membranes more susceptible to lipid peroxidation and pore formation, while normal cells are protected by a higher level of cholesterol [20–23].

The elevated expression of the membrane-bound catalase enzyme in precancerous and cancerous cells provides a crucial defense mechanism against the programmed cell death, apoptosis. Bauer et al. showed that ROS, specifically singlet oxygen, can inactivate this protective catalase, which subsequently restores the sensitivity to apoptosis induction in cancer cells.[24–26].

Cells and tissues can be exposed to plasma either directly or indirectly. The indirect method can be achieved by using plasma-activated (also referred to as plasma-treated or plasma-conditioned) liquids (PALs). When the plasma interacts with a liquid, the plasma-formed gaseous reactive species are transported through the plasma–liquid interface, leading to the formation of secondary RONS in the liquid, such as hydroxyl radicals ·OH, hydrogen peroxide H_2O_2, nitrites/ nitrates NO_2^-/NO_3^-, peroxynitrites/peroxynitrous acid, $ONOO^-$/ONOOH, peroxynitrates/peroxynitric acid O_2NOO^-/O_2NOOH, superoxide/perhydroxyl radicals $O_2{\cdot}^-$/$HO{\cdot}_2$, singlet oxygen $^1O_2$ or ozone O_3 [27–30]. The main advantage of indirect plasma treatment is the potential for minimally invasive administration through direct intratumoral injection, enabling highly targeted therapy. Intraperitoneal injections of PAL have shown antitumor efficacy against ovarian cancer, gastric cancer, pancreatic cancer and melanoma [31–35].

The potential of plasma-activated liquids extends beyond their direct cytotoxic effects. It was shown that plasma activated (cell culture) medium (PAM) significantly increased the sensitivity of breast cancer cells to paclitaxel, thereby enhancing its cytotoxic effect [36]. Therefore, besides the ability of plasma to trigger processes leading to cell death, PAL could also be used in synergy with conventional chemotherapy.

Our choice to use PBS instead of more complex cell culture media like plasma-activated media (PAM) is a well-established practice in the field, allowing better control of plasma-generated RONS. The presence of amino acids, fetal bovine serum, and pyruvate in cell culture media, can make it challenging to quantify and control RONS concentrations in PAM due to their interaction with these components [37]. These interactions can lead to a misinterpretation of the effects on cells, as demonstrated in study [38]. Using a simple stable solution such as PBS, water, or saline provides better control and a more consistent final composition [39]. Additionally, research on a lung cancer cell line found that plasma activated PBS (PAPBS) had the most significant anti-tumor effect when compared to PAM and plasma activated saline (PAS) [40].

Researchers hypothesized that plasma could reverse resistance to the drug by changing the expression of affected genes. A study on tamoxifen-resistant (TamR) MCF-7 cells showed that the direct application of cold plasma restored their sensitivity to the drug [41]. Restoration of drug sensitivity was also demonstrated in paclitaxel-resistant MCF-7 cells [42]. The mechanism of plasma-restored sensitivity in both tamoxifen resistance and paclitaxel resistance is likely based on different molecular mechanisms, as a distinct gene and network signature was identified in each of the specific resistant cell lines. Although the molecular mechanisms may differ, in both cases a significant increase in the level of intracellular ROS was detected [42].

The development of acquired drug resistance remains a major obstacle in oncology, limiting the chances of curing cancer. In this study, we investigate the potential antitumor effect of PAPBS on multidrug-resistant breast cancer cells to widely used chemotherapeutics paclitaxel, with cross-resistance to doxorubicin. Paclitaxel is a mitotic inhibitory taxane and a microtubule-stabilizing agent. The mechanism of apoptosis induction is based on beta-tubulin binding and microtubule stabilization [43]. Paclitaxel is one of the chemotherapeutics that contributes to cellular toxicity by inducing oxidative stress by regulating the activity of NADPH oxidase, thereby promoting ROS generation [44]. The objective of this study was to determine whether PAPBS can trigger processes leading to cell death in both, drug sensitive and drug-resistant cells, thereby offering a potential strategy to overcome the resistance that limits the effectiveness of conventional chemotherapies [45,46].

Despite testing a potential anti-tumor drug on 2D cell monolayers is a common methodology, the flat plastic or glass substrates used for cell culturing do not well represent the in vivo cellular environment. In this study, three-dimensional (3D) cellular models, spheroids are targeted along with 2D adherent cells. Spheroids, conversely, mimic the mechanical and biochemical properties of native tissues more accurately, including the crucial cell–cell and cell-extracellular matrix (ECM) communications, which are absent in 2D cell cultures [47].

Results

Concentration of reactive oxygen and nitrogen species in PAPBS

The concentrations of four long-lived reactive oxygen and nitrogen species (RONS) in PAPBS samples—hydrogen peroxide (H_2O_2), nitrites (NO_2^-), nitrates (NO_3^-), ozone (O_3)—were measured using colorimetric

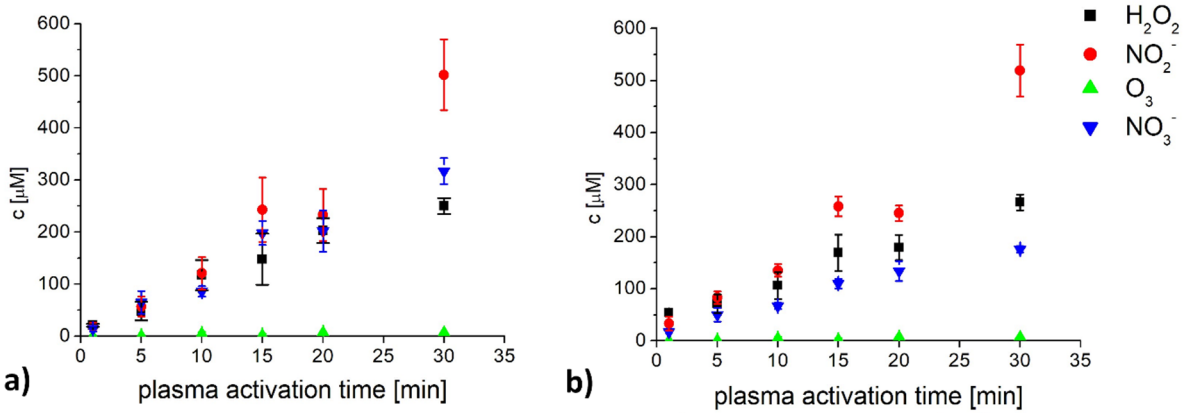

Fig. 1. Concentrations of long-lived RONS in plasma activated PBS. (**a**) Immediately after plasma exposure. (**b**) 24 h after plasma exposure. Graphs show mean concentrations ± standard deviation.

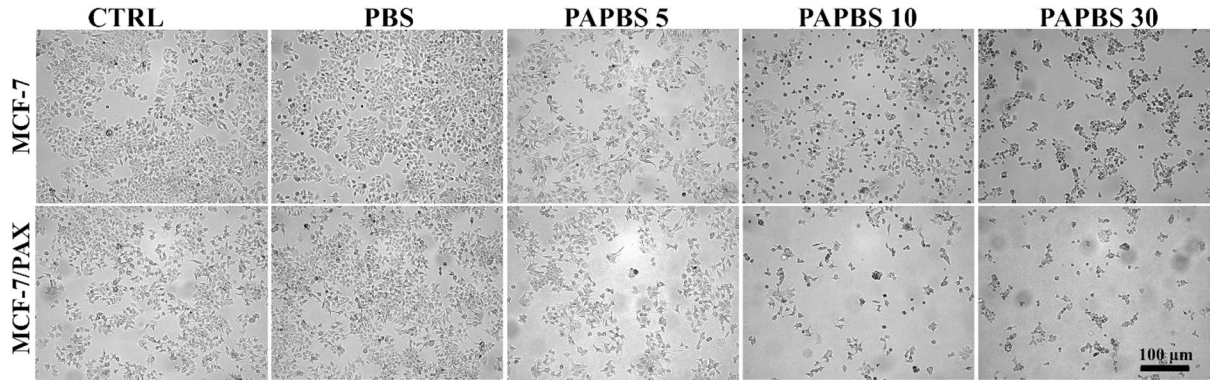

Fig. 2. Microscopic images of the breast cancer cell line MCF-7 (top), and its paclitaxel-resistant subline MCF-7/PAX (bottom) 24 h after PAPBS application. Cells in untreated culture medium and untreated PBS – control groups. Cells treated by PAPBS activated by plasma for 5, 10, 30 min. The time of PAPBS action was 1 h, after which PAPBS was replaced with the growth medium (DMEM). Scale bar = 100 µm. (Zeiss Axio Verte. A1 optical microscope). Experiments were performed in triplicate, and three independent biological replicates were conducted for each experimental condition.

methods (see Fig. 1). A 5 ml of PBS was exposed to streamer corona discharge (12.8 kV) for 1, 5, 10, 15, 20, and 30 min. Then RONS were analyzed immediately after the plasma activation of PBS and after 24 h of PAPBS storage at 37 °C. The concentrations of RONS in untreated PBS were below the limit of detection and thus served as a blank control.

The concentrations of RONS linearly increased with the plasma activation time. The seemingly decrease of RONS from 15 to 20 min in Fig. 1 a) and b) is within the experimental uncertainty. After 24 h, the RONS concentrations remained relatively stable, with only a slight decrease observed in nitrate (NO_3^-) levels. Even after 30 min of plasma activation, concentration of ozone did not increase significantly, which is due to ozone very low solubility in water solutions.

Morphological changes of MCF-7 and MCF -7/PAX cells after treatment

The effect of PAPBS on adherent breast cancer cells was observed using optical microscope 24 h after treatment, the representative photographs are shown in Fig. 2.

Untreated control cells formed nearly confluent monolayers, indicating their vital proliferation and healthy growth. They exhibited typical polygonal shapes and maintained good adherence. Compared to the control group, cells treated by PAPBS exhibited a significantly reduced cell density. The monolayer was non-confluent; the cells exhibited abnormal morphology and a loss of adherence. Apoptotic features, including cell shrinkage, rounding, and clumping, were observed starting with the PAPBS 10-min treatment, and these effects became most pronounced in cells treated with PAPBS 30-min treatment. A comparable reaction to PAPBS was observed in both drug-sensitive and drug-resistant breast cancer cells. The samples were labeled PAPBS 5, 10, 30, with 5, 10, 30 representing the plasma activation time in minutes.

Viability of breast cancer cells

Cell viability of drug-sensitive (MCF-7) and drug-resistant (MCF-7/PAX) breast cancer cells was evaluated 72 h after incubation of the cells in PAPBS. The viability of both breast cancer cell lines significantly decreased following the treatment with PAPBS treated by streamer corona discharge for 5, 10, 15, 20 and 30 min (Fig. 3). A clear dose-dependent cytotoxic effect was observed, with longer plasma activation times leading to significantly greater decreases in cell viability. A significant viability drop to 80% compared to controls was observed after incubation with PAPBS activated for 5 min, and only 40% of both breast cancer cell lines were viable after incubation in PAPBS 20. The strongest reduction in viability was observed in samples treated with PAPBS activated for 30 min. Both the drug-sensitive (MCF-7) and drug-resistant (MCF-7/PAX) cell lines exhibited comparable sensitivity to PAPBS treatment. On the other hand, incubation of the cells with PAPBS treated for 1 min seems to slightly induce the MCF-7 cell proliferation. The control groups incubated in DMEM were normalized to 100%. The decrease in viability caused by untreated PBS was negligible.

Apoptotic cell death in breast cancer cells

To assess the ability of PAPBS to induce the apoptotic cell death in breast cancer cells, Annexin V and 7-AAD staining were performed, followed by the flow cytometry analysis. Combination of these dyes allows the cells be categorized into four populations based on their membrane integrity and the externalization of phosphatidylserine—into live, early apoptotic, late apoptotic (dead), and non-apoptotic dead cells (Fig. 4).

The results demonstrate that PAPBS induces the cell death in both MCF-7 and MCF-7/PAX cells. Untreated medium and non-activated PBS were used as negative controls. In these control groups, most cells remained viable**,** at approximately 90% of the total cell population. Minimal percentages of early apoptotic, late apoptotic/dead, or debris were detected in these control groups. A significant decrease in the percentage of live cells was observed after treatment with PAPBS activated by plasma for just 10 min. With the increasing plasma activation time, the percentage of live cells decreased, while the percentage of apoptotic and dead cells increased**.** Especially with PAPBS activated for 30 min, more than 50% of cells were apoptotic.

Microscopic analysis revealed that PAPBS affects cell adhesion. Therefore, to ensure a comprehensive evaluation of the entire cell population, the detached cells from the culture medium were also collected and analyzed by flow cytometry with Annexin V staining. The results showed that most of these detached cells, in both the drug-sensitive and drug-resistant cell lines, were apoptotic (Fig. 5). As observed in the figure, the resistant cell line exhibits a higher total number of detached cells. This suggests that the resistant cells may possess slightly reduced adherence properties compared to the sensitive line.

Effect of PAPBS on the cancer cell spheroid growth

24 h after spheroid inoculation, PAPBS treatment was initiated on the fully formed spheroids. To evaluate the effects on the growth and viability of spheroids formed from drug-sensitive (MCF-7) and drug-resistant (MCF-7/PAX) breast cancer cells, four PAPBS activation times (5, 10, 20, and 30 min) and two incubation periods (1 and 24 h) were tested.

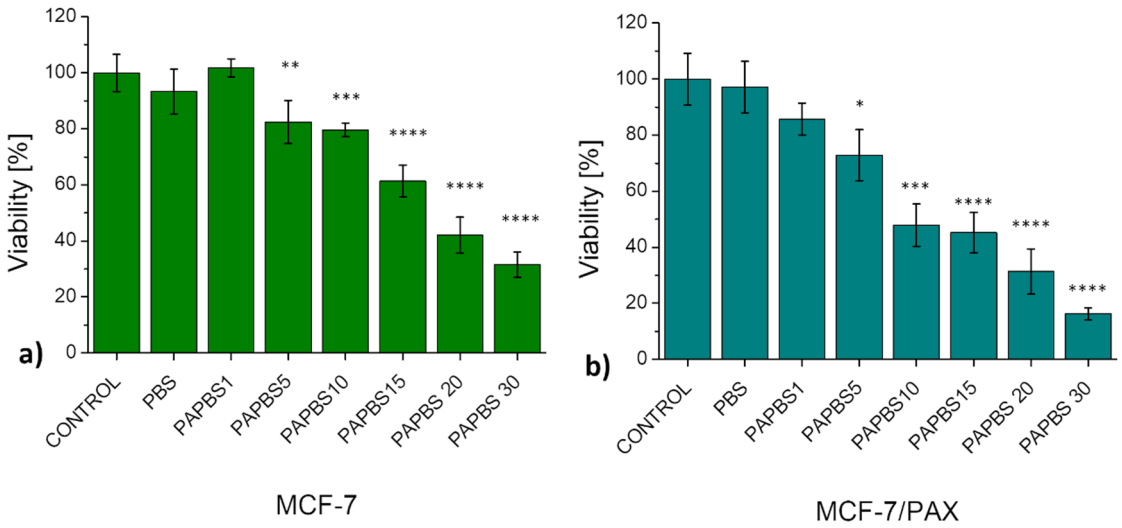

Fig. 3. Effect of plasma-activated PBS (PAPBS) on the viability of (**a**) human breast adenocarcinoma cell line MCF-7 and (**b**) its paclitaxel-resistant subline MCF-7/PAX. PBS was activated by streamer corona discharge plasma for 1, 5, 10, 15, 20, and 30 min. Cells were exposed to PAPBS for 1 h, after which it was replaced with a complete culture medium (DMEM). The effect of PAPBS was compared to controls (DMEM or PBS). Cell viability was normalized to the control group incubated in a complete medium. Error bars represent standard deviation. Statistical significance between the control and treated samples was determined using one-way ANOVA, significant changes are marked * $p < 0.05$;** $p < 0.01$;*** $p < 0.001$;**** $p < 0.0001$. Experiments were performed in sextuplicate, and three independent biological replicates were conducted for each experimental condition.

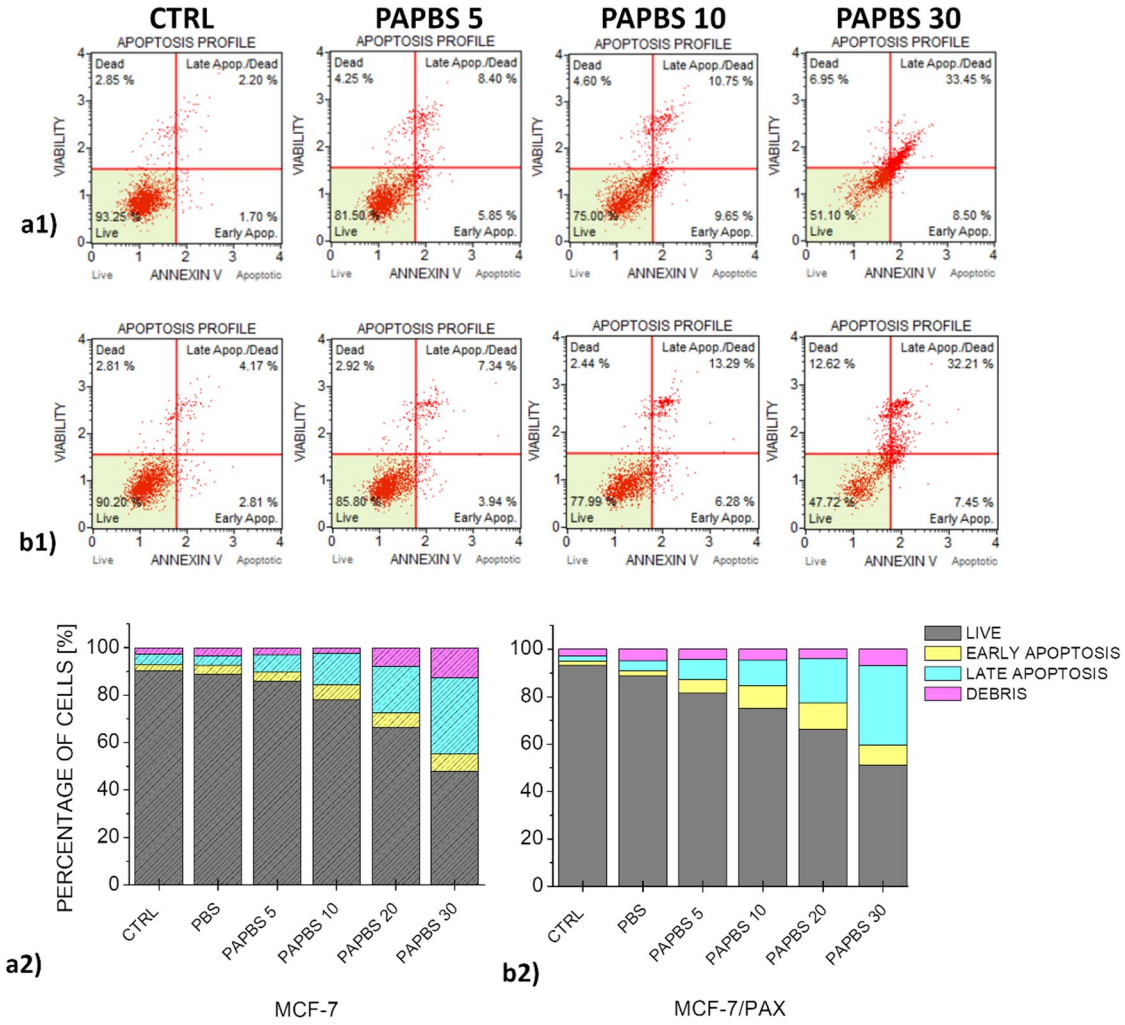

Fig. 4. Apoptosis profile of adherent (**a1**) MCF-7 and (**b1**) MCF-7/PAX obtained using Muse Annexin V & Dead Cell Assay Profiles were determined 24 h after treatment. Four quadrant markers reflected the different cellular states: the upper left quadrant contains dead cells, the upper right has late apoptotic/dead cells, the lower left contains live cells, and the lower right early apoptotic cells. Percentage of live, apoptotic and dead cells of (**a2**) MCF-7 and (**b2**) MCF-7/PAX. PBS was activated by streamer corona discharge plasma for 5, 10, 20, and 30 min. Cells were exposed to PAPBS for 1 h, after which it was replaced with a complete culture medium (DMEM). The effect of PAPBS was compared to two control groups: cells incubated in untreated culture medium and cells incubated in untreated PBS Experiments were performed in triplicate, and three independent biological replicates were conducted for each experimental condition.

1-hour PAPBS exposure

Observed on the first day post-treatment, PAPBS treatment of MCF-7 spheroids for 1 h caused a significant difference in size between the treated groups and control spheroids incubated in cell culture medium. While control spheroids grew to approximately 110% of their initial size, PAPBS-treated spheroids exhibited a significant reduction in size. PAPBS-30 caused the most significant shrinkage. Spheroids treated with untreated PBS showed only slight changes in growth when compared to the control.

By days 3 and 6 post-treatment, the control, PBS, PAPBS 5, and PAPBS 10 groups continued to grow. However, due to the initial shrinkage of the PAPBS-treated spheroids on day 1, these groups did not reach the same overall size as the controls. While control spheroids reached 133% of their initial size, the growth of PBS-treated spheroids was slightly inhibited. The PAPBS 5 and 10 spheroids reached a smaller final size, approximately 110% of their initial size.

PAPBS 20 and 30 treatments caused significant spheroid growth inhibition. By day 3 post-treatment, spheroids in both groups showed a significant reduction in size. By day 6, the PAPBS 20 spheroids slightly increased in size from their lowest point but still did not reach their initial size. PAPBS 30-treated spheroids showed a continuous decrease in size, reaching 73% of their initial size after a single 1-h exposure. The effects of a 1-h exposure to PAPBS on MCF-7 spheroid growth are shown in Fig. 6.

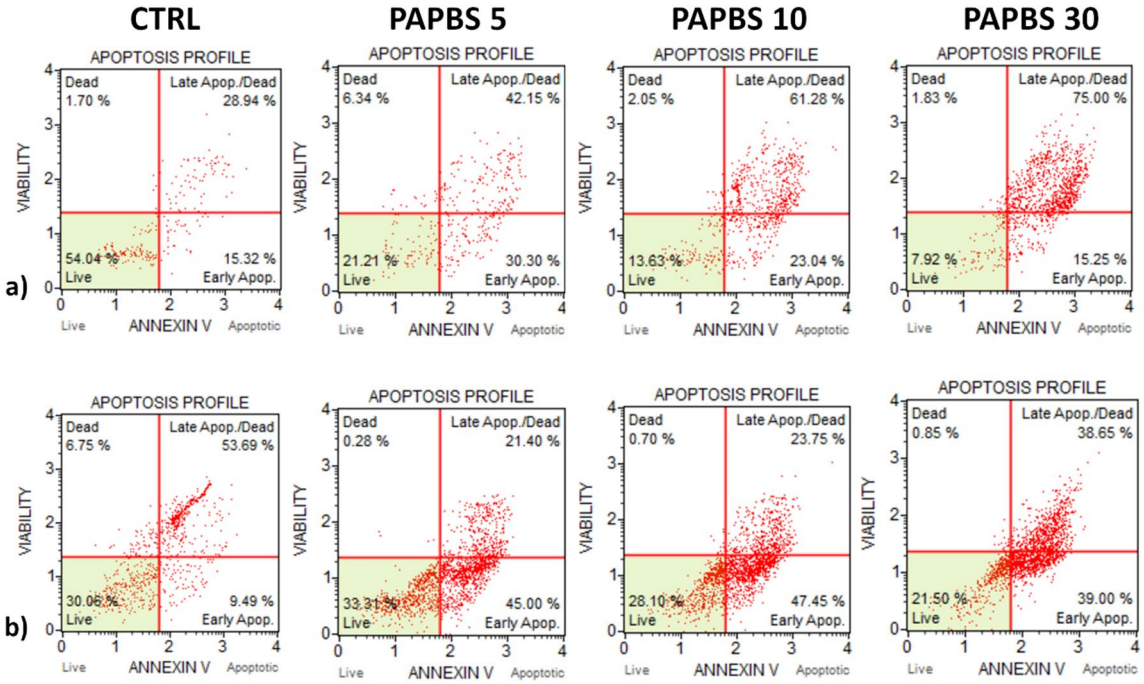

Fig. 5. Apoptosis profile of detached (**a**) MCF-7 and (**b**) MCF-7/PAX collected from the culture medium obtained using Muse Annexin V & Dead Cell Assay. Profiles were determined 24 h after treatment. Four quadrant markers reflected the different cellular states: the upper left quadrant contains dead cells, the upper right has late apoptotic/dead cells, the lower left contains live cells, and the lower right early apoptotic cells. Experiments were performed in triplicate, and three independent biological replicates were conducted for each experimental condition.

Microscopic images revealed cellular debris around spheroids treated with higher PAPBS activation times, most notably in the PAPBS 20 and PAPBS 30 groups. This debris is indicative of the loss of cellular integrity and spheroid disintegration.

Similar effects were observed on drug-resistant MCF-7/PAX spheroids after a 1-h exposure to PAPBS. Control and PBS-treated spheroids grew to approximately 130% of their initial size, while the growth of spheroids treated with PAPBS was significantly inhibited. The effects of a 1-h exposure to PAPBS on MCF-7/PAX spheroid growth are shown in Fig. 7.

24-hour PAPBS exposure

A 24-h PAPBS treatment inhibited MCF-7 spheroid growth. Surprisingly, PAPBS30 treated spheroids showed an unexpected and significant increase in size 24 h after treatment. However, by day 3, they shrunk back to their initial size, and by day 6, all PAPBS treated spheroids reached their original size. The effects of a 24-h exposure to PAPBS on MCF-7 spheroid growth are shown in Fig. 8.

This phenomenon was even more pronounced in MCF-7/PAX spheroids. After a 24-h incubation with PAPBS 30, these spheroids grew dramatically and then shrank. The spheroids became very fragile with a loss of structural integrity, a visibly altered core, and irregular, rough edges. The effects of a 24-h exposure to PAPBS on MCF-7/PAX spheroid growth are shown in Fig. 9.

Viability of spheroids after PAPBS exposure

1-hour PAPBS exposure

Spheroid viability after PAPBS exposure was evaluated using a CellTiter-Glo® luminescent cell viability assay, with analysis performed 72 h after treatment. For MCF-7 spheroids, a significant decrease in viability to approximately 80% was observed after 1-h exposure only with the higher doses PAPBS 20 and 30 (Fig. 6). In contrast, drug-resistant MCF-7/PAX spheroids were more sensitive, with viability starting to decrease already with PAPBS 5, dropping to approximately 72%. The highest dose, PAPBS 30, drastically reduced the viability to just 18% (Fig. 7).

24-hour PAPBS exposure

A dose-dependent decrease in the viability of MCF-7 spheroids was observed after a 24-h PAPBS exposure. Viability decreased from 77% after the PAPBS 5 treatment to 63% after the PAPBS 30 treatment (Fig. 8). For MCF-7/PAX spheroids, while the untreated PBS group demonstrated a slight increase in viability to 113%, PAPBS 10 reduced viability to approximately 67%. The highest doses, PAPBS 20 and 30, caused a dramatic reduction in viability to about 54% and 1% respectively, indicating that the PAPBS 30 treatment resulted in non-

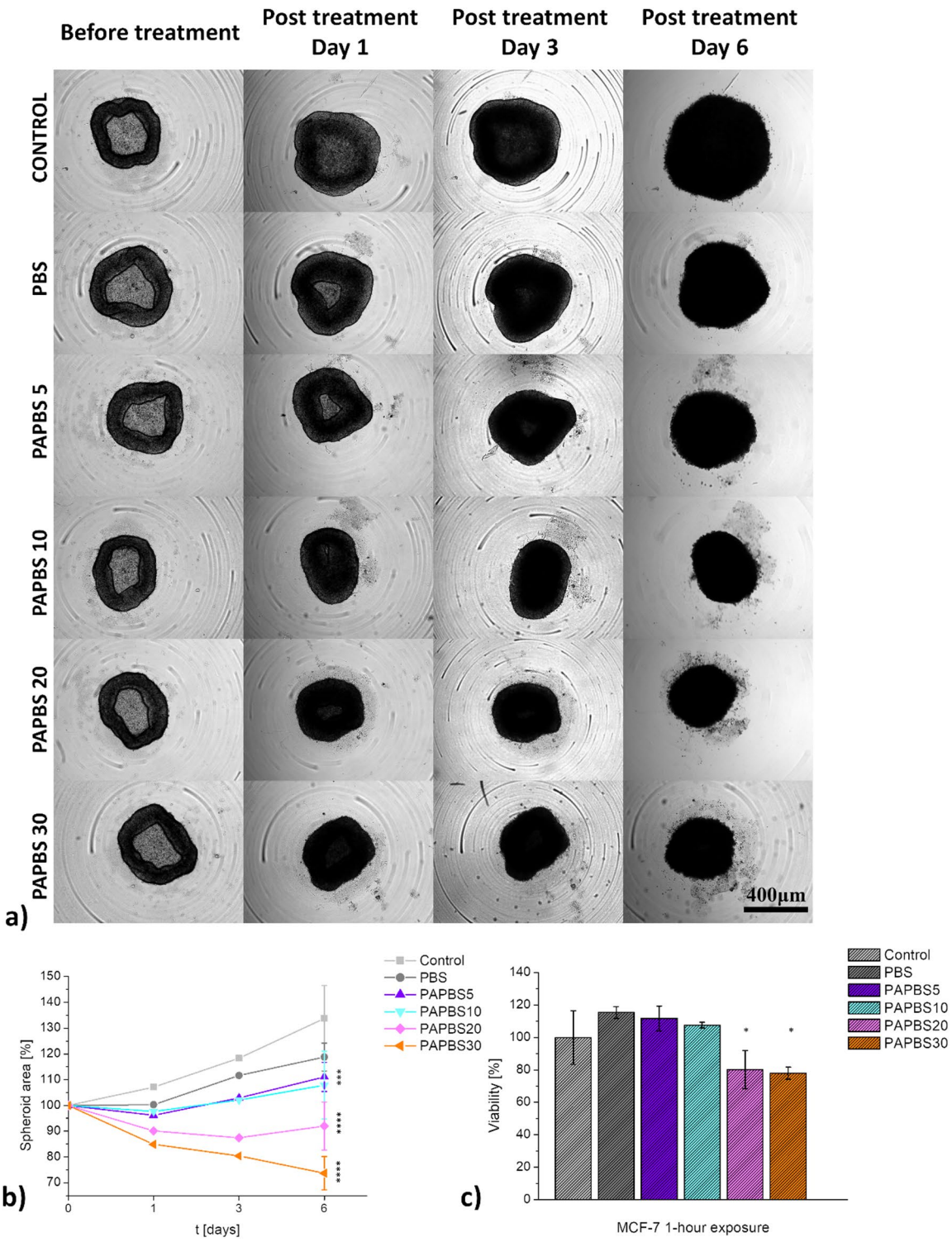

Fig. 6. Effect of PAPBS on MCF-7 spheroid growth and viability after 1-h PAPBS treatment. Two control groups were used: spheroids cultured in untreated growth medium and in untreated PBS. Spheroids treated by PAPBS activated by plasma for 5, 10, 20, 30 min. a) Microscopic images of individual spheroids before treatment, and at 1, 3, and 6 days after treatment. Scale bar = 400 µm. (Zeiss Axio Verte.A1 optical microscope). b) Relative change in spheroid area over 6 days. The initial spheroid area on Day 0 was normalized to 100%. The area at subsequent post-treatment days (1, 3, and 6) was calculated as a percentage of its own initial area. The data shown represent the average of these individual percentage changes (12 spheroids per treatment group). c) Viability of spheroids measured by CellTiter-Glo® assay 3 days after treatment. Viability of control group was normalized to 100% (3 spheroids per treatment group). Statistical significance between the control and treated samples was determined using one-way ANOVA, significant changes are marked * $p < 0.05$;*** $p < 0.001$;**** $p < 0.0001$. Experiments were performed in sextuplicate, and three independent biological replicates were conducted for each experimental condition.

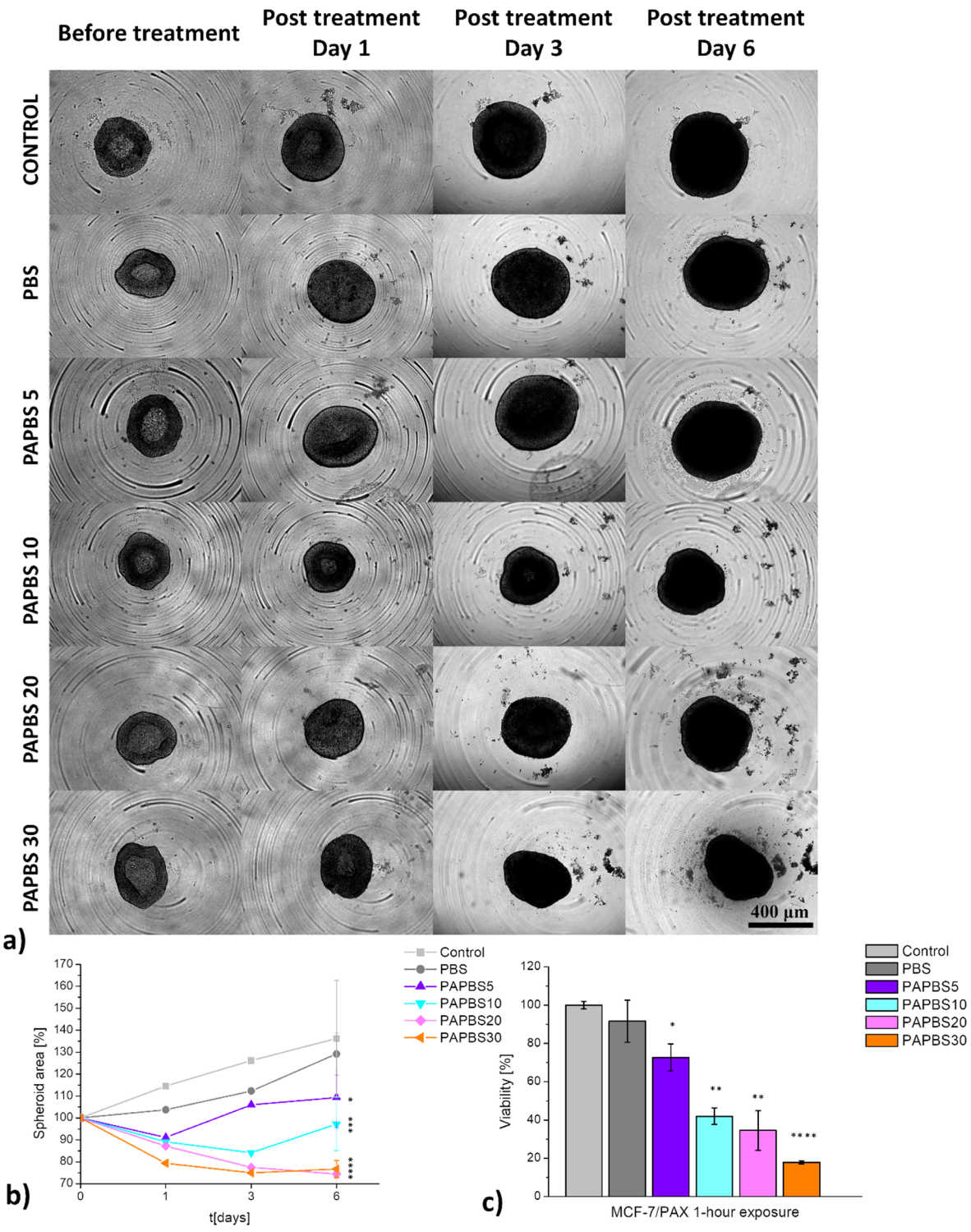

Fig. 7. Effect of PAPBS on paclitaxel resistant MCF-7/PAX spheroid growth and viability after 1-h PAPBS treatment. Two control groups were used: spheroids cultured in untreated growth medium and in untreated PBS. Spheroids treated by PAPBS activated by plasma for 5, 10, 20, 30 min. a) Microscopic images of individual spheroids before treatment, and at 1, 3, and 6 days after treatment. Scale bar = 400 µm. (Zeiss Axio Verte.A1 optical microscope). b) Relative change in spheroid area over 6 days. The initial spheroid area on Day 0 was normalized to 100%. The area at subsequent post-treatment days (1, 3, and 6) was calculated as a percentage of its own initial area. The data shown represent the average of these individual percentage changes (12 spheroids per treatment group). c)Viability of spheroids measured by CellTiter-Glo ® assay 3 days after treatment. Viability of control group was normalized to 100% (3 spheroids per treatment group). Statistical significance between the control and treated samples was determined using one-way ANOVA, significant changes are marked * $p < 0.05$;** $p < 0.001$;*** $p < 0.001$;**** $p < 0.001$. Experiments were performed in sextuplicate, and three independent biological replicates were conducted for each experimental condition.

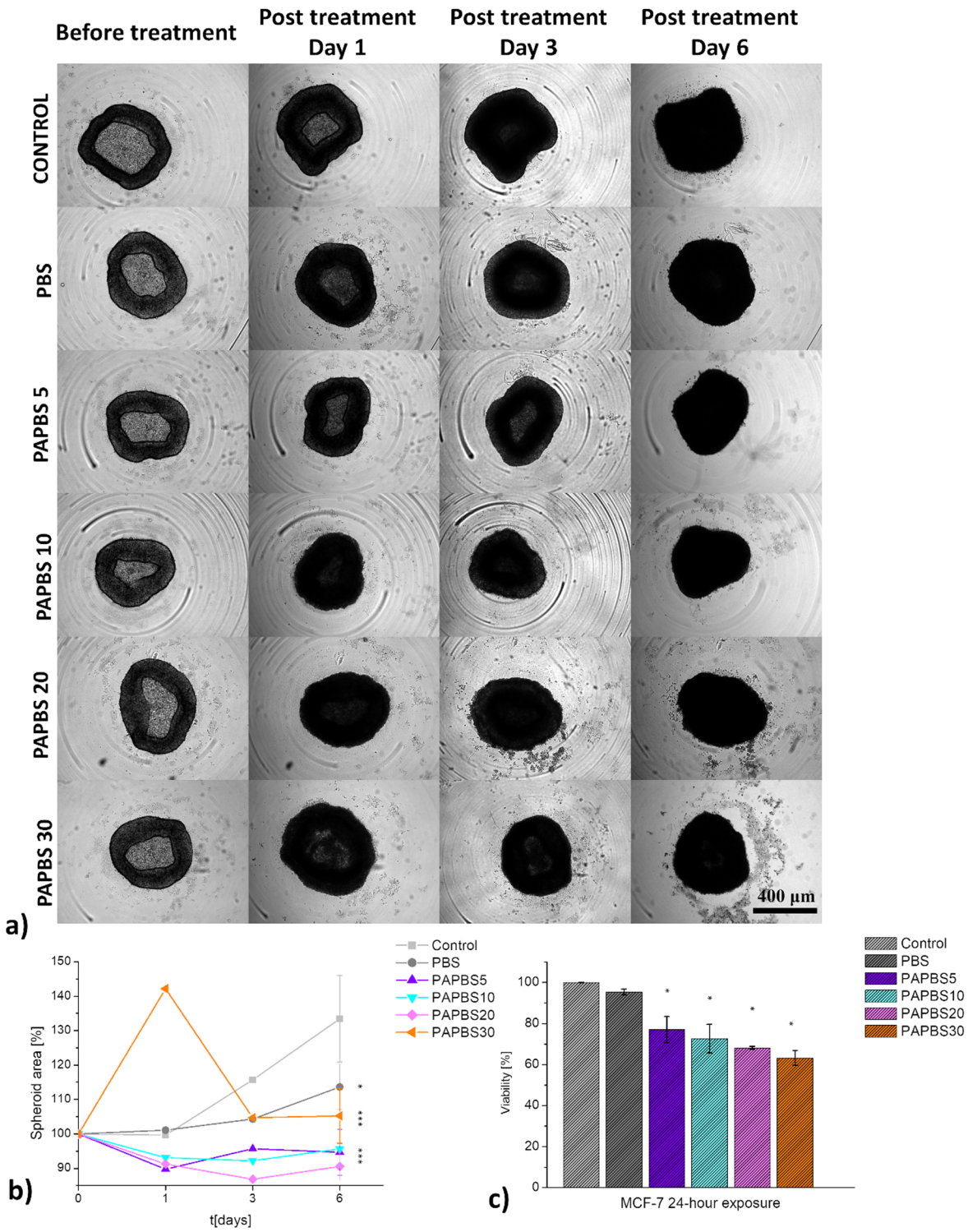

Fig. 8. Effect of PAPBS on MCF-7 spheroid growth and viability after 24-hour PAPBS treatment. Two control groups were used: spheroids cultured in untreated growth medium and in untreated PBS. Spheroids treated by PAPBS activated by plasma for 5, 10, 20, 30 min. (**a**) Microscopic images of individual spheroids before treatment, and at 1, 3, and 6 days after treatment. Scale bar = 400 µm. (Zeiss Axio Verte.A1 optical microscope). (**b**) Relative change in spheroid area over 6 days. The initial spheroid area on Day 0 was normalized to 100%. The area at subsequent post-treatment days (1, 3, and 6) was calculated as a percentage of its own initial area. The data shown represent the average of these individual percentage changes (12 spheroids per treatment group). (**c**)Viability of spheroids measured by CellTiter-Glo® assay 3 days after treatment. Viability of control group was normalized to 100% (3 spheroids per treatment group). Statistical significance between the control and treated samples was determined using one-way ANOVA, significant changes are marked ** $p < 0.01$; **** $p < 0.0001$. Experiments were performed in sextuplicate, and three independent biological replicates were conducted for each experimental condition.

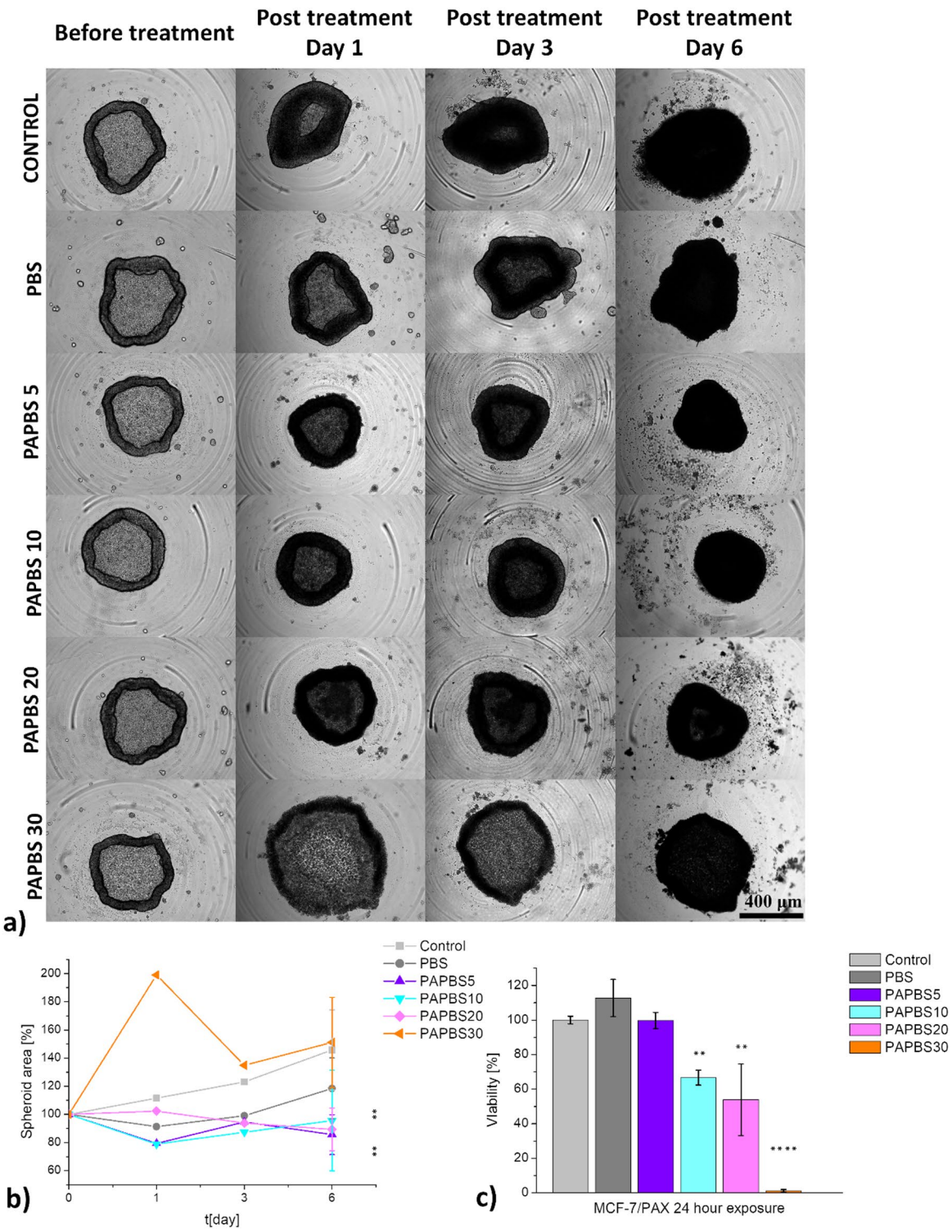

Fig. 9. Effect of PAPBS on paclitaxel resistant MCF-7/PAX spheroid growth and viability after 24-hour PAPBS treatment. Two control groups were used: spheroids cultured in untreated growth medium and in untreated PBS. Spheroids treated by PAPBS activated by plasma for 5, 10, 20, 30 minutes. a) Microscopic images of individual spheroids before treatment, and at 1, 3, and 6 days after treatment. Scale bar = 400 µm. (Zeiss Axio Verte.A1 optical microscope). b) Relative change in spheroid area over 6 days. The initial spheroid area on Day 0 was normalized to 100 %. The area at subsequent post-treatment days (1, 3, and 6) was calculated as a percentage of its own initial area. The data shown represent the average of these individual percentage changes (12 spheroids per treatment group). c)Viability of spheroids measured by CellTiter-Glo ® assay 3 days after treatment. Viability of control group was normalized to 100 % (3 spheroids per treatment group). Statistical significance between the control and treated samples was determined using one-way ANOVA, significant changes are marked ** $p<0.01$; **** $p<0.0001$. Experiments were performed in sextuplicate, and three independent biological replicates were conducted for each experimental condition.

viable spheroids (Fig. 9). Control spheroids had a dense and compact structure, the edges remained smooth and well-defined. On the other hand, the edges of PAPBS-treated spheroids were less defined and showed signs of cellular disintegration and a presence of cellular debris. The core of spheroids treated by PAPBS 5 appears less compact. In case of PAPBS 30, the core is noticeably disrupted and appears sparse, indicating extensive cell death and loss of integrity (Fig. 10).

Discussion

This study investigates the effects of plasma-activated phosphate-buffered saline (PAPBS) on human breast adenocarcinoma cell lines in 2D cell monolayers and 3D spheroids. By comparing responses of paclitaxel-sensitive MCF-7 cancer cell line with its paclitaxel-resistant subline, MCF-7/PAX, we examined the potential of PAPBS as an anticancer therapy for breast cancer, even when tumors develop resistance to conventional treatments.

It should be noted that in this study, indirect plasma effects were tested via plasma-activated liquid. The PBS was plasma-treated in a separate step before being transferred to the cell cultures. The cells were not directly exposed to plasma discharge, inherently eliminating any direct effects from UV radiation or electric fields.

The activation of PBS using a streamer corona discharge generated by a portable plasma pen successfully produced various reactive oxygen and nitrogen species (RONS), as previously described in earlier studies [48,49]. The concentration of H_2O_2, NO_2^- and NO_3^- increased with the plasma treatment time ('dose') and remained relatively stable for at least 24 h at 37 °C. This is consistent with a study that tested the stability of PAPBS at room temperature and its effect on cell cytotoxicity, reporting no changes after 2 h [50]. Extended stability of PAPBS represents a significant practical advantage, potentially allowing for the preparation of a liquid anticancer agent one day in advance of clinical application.

We investigated a range of plasma activation times from 1 to 30 min, with detailed focus on the 5, 10, 20, and 30-min treatments that yielded the most significant anti-tumor effects. PBS treatment (activation) was not extended beyond 30 min because prolonged exposure led to a substantial volume reduction from evaporation. For instance, a 30-min treatment resulted in a 10% volume loss (500 µl from an initial 5 ml), which could lead to a more concentrated solution.

Microscopic observations of breast cancer cells treated with PAPBS confirmed a reduction in viable cells and significant morphological changes in both drug-sensitive and drug-resistant lines. Decrease in viability, also confirmed by metabolic assay, cannot be attributed to the temporary absence of nutrients, as cells incubated in untreated PBS did not show a similar reduction. The observed morphological changes are consistent with those reported in a separate study that investigated direct and indirect plasma-activated medium (PAM) treatment on various non-metastatic and metastatic breast cancer cells [51]. PAM induced similar or even higher cytotoxicity when compared to direct plasma treatment. The anti-cancer effects observed were attributed to the triggering of apoptosis and the regulation of key tumor microenvironment effectors, such as ROS, matrix receptors, proteases, and inflammatory mediators.

Further analysis using flow cytometry proved that PAPBS induced apoptosis in MCF-7 cells, with a comparable induction rate also evident in the paclitaxel-resistant MCF-7/PAX subline. PAPBS primarily triggers an apoptotic pathway, rather than immediate necrosis. While untreated PBS proved to be non-toxic to cells, the cytotoxicity of PAPBS is mediated by the RONS generated during the plasma activation of the liquid.

The effects of liquids activated by the same plasma source have been previously studied on melanoma, glioblastoma, and pancreatic cancer cells [49]. After 30-min incubation of cancer cells in plasma activated medium (PAM) or PAPBS, a significant decrease in viability and apoptosis induction were detected. The same plasma dose did not trigger apoptosis in normal cells, indicating a selective antitumor effect.

The efficacy and selectivity of PAL is further supported by an in vivo study, where PAL containing similar RONS concentrations to those detected in this study, was found to inhibit the growth of melanoma, lung, and oral tongue squamous tumors. Importantly, this treatment did not cause harmful effects on liver, kidney, or myocardium function [52].

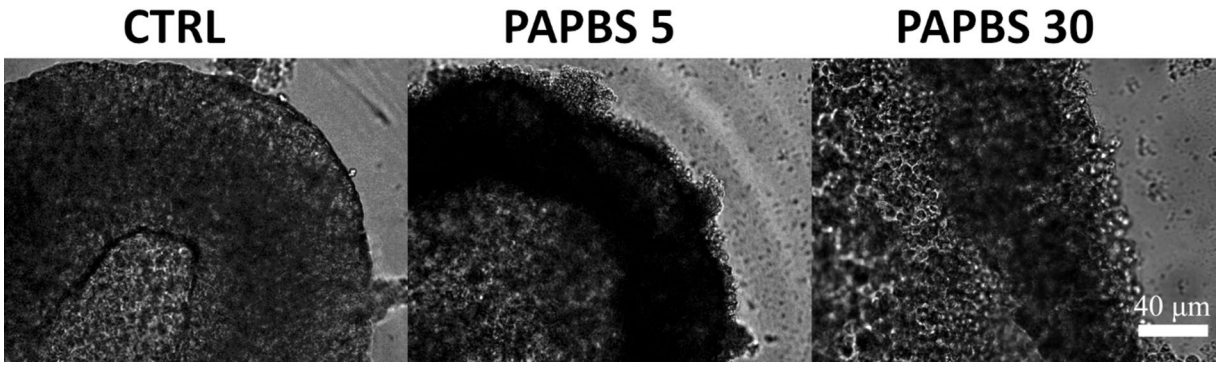

Fig. 10. Detailed microscopic images of MCF-7/PAX spheroid after 24-hour PAPBS treatment. PAPBS were treated for 5 and 30 minutes, control spheroids were cultured in untreated growth medium. Images were taken on day 1 post-treatment. Scale bar = 40 µm. (Zeiss Axio Verte.A1 optical microscope).

A correlation between the concentration of RONS in the PAPBS samples and the reduction in cell viability was observed, supporting the conclusion that RONS play the main role in mediating the cytotoxic effects of indirect plasma treatment. The efficacy of PAPBS in reducing cell viability in dose-dependent manner is consistent with numerous studies that have shown the anti-tumor effects of plasma-activated PBS on various cell lines [40,49,50,53].

Multiple studies have found that H_2O_2 is an essential, but not sufficient trigger of cell toxicity [49,50,53,54]. Synergistic effect between H_2O_2 and NO_2^- was demonstrated in glioblastoma, melanoma and colorectal cancer cell lines. Although the addition of NO_3^- to H_2O_2 and NO_2^- did not significantly increase cytotoxicity, we cannot discount that NO_3^- and other reactive species play a role in the anti-tumor activity of PAPBS [50,54].

To provide a more accurate representation of real tumor behavior, in addition to 2D cell monolayers, we also studied 3D tumor models formed from the same human breast adenocarcinoma cells, both paclitaxel-sensitive (MCF-7) and resistant (MCF-7PAX). All PAPBS-treated spheroids showed inhibition of growth or shrinkage, in contrast to the controls and untreated PBS-incubated spheroids which grew. Low plasma doses, PAPBS 5 and 10 incubated for 1 h with spheroids, induced an acute reduction in spheroid size, which was most pronounced one day post-treatment. In the following days, their growth curves were similar to those of the control group. This growth rate is also demonstrated in a study evaluating the combined application of PAPBS and pulsed electric fields on spheroids formed from colorectal carcinoma cells [55]. The high-dose PAPBS treatment resulted in the most dramatic visual change of spheroids, demonstrating a dose-dependent effect of PAPBS on spheroid growth, from mild inhibition at low doses to continuous shrinkage at high doses. Spheroids were significantly reduced in size and were surrounded by a large amount of cellular debris, indicating severe cytotoxic effects.

We also observed some cell spreading after the PAPBS treatment. Since PAPBS can cause a loss of cellular adherence, there is a potential risk of metastasis if these detached cells remain viable. However, we assessed the viability of these detached cells in 2D monolayers using Annexin V staining and found that the majority were either apoptotic or dead.

Our findings are consistent with a previous study, which tested antitumor effect of PAM on MCF-7 spheroids [36]. While their study used a different plasma source and a much smaller volume of liquid, our results on spheroid growth were similar. This demonstrates that comparable effects can be achieved with different plasma sources and emphasizes the necessity of characterizing the concentration of RONS to define the plasma dose and ensure consistent outcomes across various experimental setups. Apoptosis induction and inhibition of tumor growth caused by PAPBS were also demonstrated in 2D and 3D models of pancreatic cancer [56].

Microscopic analysis revealed that all spheroids exposed to PAPBS treatment exhibit a noticeable darkening of their core. These changes can reflect the formation and propagation of the necrotic core or it can be attributed to an increase in cellular density, supporting the theory that the reduction in spheroid size could be caused by a decrease in intercellular space**.** This enhanced compaction and reduction in size could be clinically beneficial, as it may potentially make the tumor easier to be surgically resected.

Previous study has shown that a 24-h incubation in PBS has a significant harmful effect on the viability of 2D cell monolayers across various cell lines [49]. In 2D monolayers, all cells are directly and uniformly exposed to the PAPBS treatment. In contrast, the 3D structure creates layers where cells on the surface and cells in the necrotic or quiescent core are affected differently. Therefore, it was essential to test whether PBS alone would induce spheroid shrinkage or structural disintegration. Demonstrating that the spheroids remain structurally intact in PBS confirms that the observed cytotoxic effects in subsequent experiments are a result of the treatment (PAPBS) rather than simple starvation. A longer 24-h exposure was necessary to allow the RONS to penetrate the deeper layers of the spheroid. Using the same exposure for both 2D and 3D models would either lead to total 2D cell death or insufficient 3D penetration in spheroids. With respect to the potential clinical use of PAPBS for cancer treatment, we considered it important to test spheroids which are better 3D tumor models in conditions when the effect was observed, even though these conditions were not identical with 2D monolayers.

The morphological changes observed in tumor spheroids, specifically the swelling after 24 h of incubation with PAPBS 30, represent a novel finding. The spheroids appeared larger and exhibited a loss of compactness which can be attributed to the changes in cell–cell interaction and the inhibition of adherens junctions. This interpretation correlates with our previous 2D monolayer demonstration, showing that PAPBS treatment induced a clear loss of cell adherence.

This phenomenon is similar to the spheroid swelling documented in studies where it was induced by hyperthermia [57]. The authors of the study described two mechanisms that could be responsible for the increase of spheroidal volume. The first mechanism proposes that the increase in spheroidal volume is a direct result of changes in the volume and shape of individual cells. Given that the spheroids in our study are composed of a large number of cells (starting from 4×10^4), the swelling of each individual cell would cumulatively lead to a significant increase in the overall spheroid volume. The second explanation is based on changes in the organization of the extracellular matrix (ECM), which causes a reorganization of cell packing density and a subsequent expansion of the intercellular space.

Cell swelling typically occurs in a hypoosmotic liquid due to an influx of water, however, this mechanism can be discounted in our study, as PBS is an isotonic solution. The plasma activation of the PBS likely increases its osmolarity [53], which could explain the significant spheroid shrinkage without a dramatic decrease in viability observed at lower plasma activation times, especially in MCF-7 spheroids. In this case, the RONS concentration was likely too low to cause significant cellular damage in more stable cellular model compared to 2D cell monolayers, and the visible effect could be an osmotic response or reorganization of cell packing density.

Another potential explanation of spheroid swelling is that while cells undergoing apoptosis shrink and condense, on the other hand, the cell death marked by cellular swelling is known as oncosis [58,59]. This increase in the volume of individual cells could lead to an increase in the overall volume of the spheroid.

Interestingly, massive spheroid swelling and a decrease in spheroid viability to 0% compared to the control group was observed especially in the paclitaxel-resistant breast cancer line. A variability in the response of

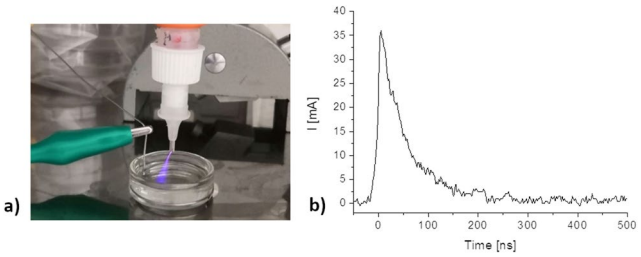

Fig. 11. (**a**) Plasma activation of PBS by streamer corona discharge. (**b**) One current pulse of corona discharge measured by a current probe (Pearson 2878) and an oscilloscope (Tektronix TDS2024).

spheroids formed from different cell lines to the effect of PAPBS has also been demonstrated in a study that tested plasma-activated liquids on 3D colorectal and ovarian cancer spheroids. This research, which focused on PAPBS and plasma-activated saline (PAS), showed that PAPBS was more efficient than PAS. While both liquids induced apoptosis in the peripheral cells of the spheroids, PAPBS affected cells in deeper layers and caused more rapid cell death [53].

Our observation that PAPBS is effective against the paclitaxel-resistant MCF-7/PAX cell line is a significant and promising finding. Even chemotherapeutic drug-resistant tumors could be efficiently potentially treated by the new modality represented by PAPBS.

Material and methods

Plasma activation of PBS

The phosphate-buffered saline (PBS, Dulbecco A, OXOID, Basingstoke, UK) was activated using a portable plasma pen, which generates a DC-positive streamer corona in ambient atmospheric air between the tip of the needle electrode and the surface of the treated liquid. The distance between the needle electrode tip and the surface of the liquid was kept 1 cm throughout all treatments. A direct current voltage of 12.8 kV was applied to the needle electrode. The second electrode was a grounded wire immersed in the treated liquid. The streamer discharge used was self-pulsing with a maximum amplitude of 30–40 mA per pulse and an average frequency of 10 kHz. The electrical parameters of the discharge were measured using a current probe (Pearson 2878) and an oscilloscope (Tektronix TDS2024) (Fig. 11).

The PBS was placed in a glass Petri dish (40 mm in diameter) with a volume of 5 ml in each session. The liquid was exposed to plasma at various time intervals (1, 5, 10, 15, 20 and 30 min) to obtain different concentrations of long-lived reactive oxygen and nitrogen species in the plasma-activated PBS (PAPBS) samples. The aim of this procedure is to optimize the plasma dose to ensure an antitumor effect while being selective toward tumor cells and gentle on healthy tissues.

Physico-chemical changes of PBS after plasma treatment

pH values of untreated PBS and PAPBS treated for 1, 5, 10, 15, 20, and 30 min measured by pH probe (WTW SenTix 60) are shown in Fig. S1 in Supplementary material. They confirm that the pH of the PBS remains stable after plasma activation. Specifically, after 20 and 30 min of treatment, the pH decreased only slightly to 6.95 and 6.85, respectively. These values remain within a biologically acceptable range, suggesting that the observed cytotoxicity is not a result of excessive acidification.

Electrical conductivity that determines osmolality of untreated PBS and PAPBS activated for 1, 5, 10, 15, 20, and 30 min measured by Greisinger Electronic GMH 3430We probe are shown in Fig. S2 in Supplementary material. The electrical conductivity of the samples increased proportionally with the treatment duration, from an initial value of 6.0 mS/cm to 6.60 mS/cm after 30 min of plasma treatment, indicating the successful enrichment of the solution with plasma-derived species.

Detection of RONS in PAPBS

Four long-lived reactive oxygen and nitrogen species (RONS) were measured in PAPBS samples using colorimetric methods measured by a UV/VIS absorption spectrophotometer (UV-1900 Shimadzu).

Hydrogen peroxide (H_2O_2)

The concentration of hydrogen peroxide was determined using titanium oxysulfate assay ($TiOSO_4$). As a result of the reaction between H_2O_2 generated in the PAPBS and $TiOSO_4$ yellow-colored compound of pertitanic acid H_2TiO_4 is formed, with the absorption maximum at 407 nm. The concentration of H_2O_2 is proportional to the absorbance [60]. Calibration curve can be found in the supplementary material (Fig. S3).

Nitrite (NO_2^-)

The concentration of nitrites was measured using Griess assay (Nitrate/Nitrite Colorimetric Assay Kit #780,001 Cayman Chemicals). Griess Reagents convert nitrite into a purple azo chromophore determines with an absorption maximum at 540 nm. Calibration curve can be found in the supplementary material (Fig. S4).

Nitrate (NO_3^-)
The concentration of nitrates was evaluated spectrophotometrically with a commercial Spectroquant® nitrate assay kit (Merck Chemicals) sulfuric and phosphoric solution nitrate ions react with 2,6-dimethylphenol (DMP) to form 4-nitro-2,6-dimethylphenol that is determined with the absorption maximum at 330 nm. To prevent interference from nitrite, amidosulfuric (sulfamic) acid was added to the samples (50 mg /10 ml of sample). Calibration curve can be found in the supplementary material (Fig. S5).

Ozone (O_3)
The presence of dissolved ozone in plasma activated PBS was performed by the Indigo blue assay based on the principle that ozone oxidizes and decolorizes the dye. The decrease of absorbance at 600 nm correlates directly with the concentration of O_3.

Cell culture and cultivation

To investigate the effects of plasma-activated PBS, two human adherent cancer cell lines were used: MCF-7 (ATCC®, HTB-22TM) cell line, derived from human breast adenocarcinoma and the MCF-7/PAX subline which exhibits resistance to paclitaxel (Division of Cell and Molecular Biology, Third Faculty of Medicine, Charles University, Czech Republic) [45,46]. This sub-line was developed by progressively exposing the original cell line MCF-7 to higher levels of paclitaxel. MCF-7/PAX subline was selected as a well-described multidrug-resistant (MDR) cell line. Both cell lines were cultivated in Dulbecco's Modified Eagle's medium—high glucose (DMEM; Sigma Aldrich, Germany, D6429) supplemented with 10% fetal bovine serum (FBS) or the resistant MCF-7/PAX cells, the medium was further supplemented with 300 nM paclitaxel to ensure the maintenance of resistance. Cell cultures at passage number 15–40 were incubated at 37 °C with 5% CO2 in a 95% humidified atmosphere (Thermo Fisher Scientific). For experiments, cells were seeded without paclitaxel into 96-well or 6-well plates, depending on the type of cell analysis.

Effect of PAPBS on cell viability in 2D condition

Cell exposure to PAPBS
Both cell lines were inoculated at 1×10^4 cells per well into 96-well plates (TPP, Switzerland) to 100 µL final volume 24 h before the exposure of plasma-activated PBS. After 24 h, the medium was replaced with 100 µL of various PAPBS samples for 1 h under standard incubation conditions. After the incubation period, the PAPBS was replaced with fresh complete cell culture medium, and the cells were further incubated for 72 h. This time point was selected to allow the differences between the untreated control and the treated groups to become more pronounced, which is essential for accurately comparing lower-dose groups with the control. To ensure comparability, the cytotoxic effects of PAPBS were tested in relation to two control groups: the first one was the control group of cells incubated in complete untreated culture medium (DMEM, supplemented with 10% FBS) and the second control group were cells incubated in untreated PBS under identical conditions.

Morphological changes and cell confluency were monitored by a microscope Zeiss Axio Verte.A1 (Zeiss, Jena, Germany) with a CCD camera Axiocam Icc 1 A1 (Zeiss, Jena, Germany) with Axio Vision software (Zeiss, Jena, Germany, version 4.8, 2011).

Cell viability assay
Cell viability following PAPBS treatment was determined using the colorimetric cell proliferation WST-1 assay (water-soluble tetrazolium salt, Roche), which is based on the enzymatic reduction of WST-1 (4-[3-(4-iodophenyl)-2-(4-nitrophenyl)-2H-5-tetrazolio]-1,3-benzenedisulfonic acid sodium salt) into formazan by mitochondrial dehydrogenases in metabolically active cells. The concentration of formazan is directly proportional to the number of viable cells. After 72 h of incubation cells in PAPBS, 5 µl of WST-1 reagent was added to each well of a 96-well plate containing 100 µl of complete culture medium. Cells were incubated with the reagent at 37 °C, 95% humidity, and 5% CO_2 atmosphere in the incubator for 3 h. After 3 h, the absorbance of the formazan was measured at 450 nm wavelength using microplate reader The BioTek Synergy HTX. The percentage change in the number of viable cells was calculated relative to the absorbance of untreated control cells.

Apoptosis assay
4×10^5 cells per well in 6-well plates were seeded to 2 ml final volume 24 h before the exposure of plasma-activated PBS. After 24 h, the medium was replaced with 1 ml of PAPBS samples (activated 5, 10, 20 or 30 min) and untreated PBS for 1 h under standard incubation conditions. After the incubation period, the PAPBS and PBS were replaced with 2 ml of fresh complete cell culture medium, and cells were further incubated for 24 h.

The percentage of apoptotic cells was determined using a Muse Annexin V & Dead Cell Kit and a flow cytometer Muse Cell analyzer (Luminex, Austin, TX, USA) with the use of fluorescent dyes Annexin V and 7-aminoactinomycin D (7-AAD). Following 24-h incubation, both adherent and detached cells were collected to ensure that the entire cell population was evaluated. Adherent cells were harvested by trypsinization and resuspended in fresh culture medium. The detached cells from the medium were centrifuged to form a cell pellet, then the supernatant was carefully removed, and the cell pellet was resuspended in culture medium to a final concentration 1×10^5cells/ml. For staining, 100 µl of the cell suspension was added to 100 µl of the Muse Annexin V & Dead Cell reagent according to the manufacturer's instructions. Before being analyzed on the Muse Cell Analyzer samples were incubated for 20 min in the dark at room temperature. Annexin V stains phosphatidylserine expressed on the outer surface of the cell membrane during apoptosis. 7-AAD penetrates dead and late apoptotic cells. The combination of these two fluorescent dyes is used to classify cells into:

non-apoptotic live—7-AAD negative, phosphatidylserine negative;
non-apoptotic dead—7-AAD positive, phosphatidylserine negative;

early apoptotic—7-AAD negative, phosphatidylserine positive;
late apoptotic, dead—7-AAD positive, phosphatidylserine positive.

Effect of PAPBS on 3D tumor models of breast cancer cells

Spheroid inoculation

For spheroid inoculation, U-bottom 96-well plates (Guangzhou Jet Bio-Filtration Co., Ltd., China) covered with a microlayer of SeaKem LE® agarose (Lonza, Switzerland) were used. Both cell lines MCF-7 and MCF-7/PAX were inoculated at 4×10^4 cells per well into per well to 100 µl final volume 24 h before the exposure of plasma-activated PBS.

Spheroid exposure to PAPBS

In each experiment, spheroids were divided into six experimental groups: control spheroids, a PBS group, and four PAPBS treatment groups with varying plasma activation times (5, 10, 20, and 30 min). Each group contained a minimum of 12 spheroids. After 24 h, when spheroids were formed, 70 µl of medium was carefully replaced with 70 µl of PAPBS samples and incubated for 1 h or 24 h at 37 °C, 95% humidity, and a 5% CO_2 atmosphere. After the incubation time, the 70 µl of volume in each well was carefully replaced with fresh complete medium, and the cells were incubated for an additional 6 days. Control spheroids underwent the same liquid exchange as PAPBS-treated samples but only using culture medium.

Spheroid growth

Shape and growth of spheroids were evaluated using an optical microscope (Zeiss Axio Verte.A1 with a CCD camera Axiocam Icc 1 A1 with Axio Vision software. Spheroid area was measured before treatment (day 0) and on days 1, 3, and 6 post-treatment.

The measured area corresponds to the 2D circular area visible in the microscopic images. The size was determined by analyzing these 2D projections using ImageJ software. To ensure accuracy, the pixel-to-micrometer conversion was calibrated based on the scale bar generated by the AxioVision software. The final area was then expressed in square micrometers (μm^2).

The growth of each individual spheroid was calculated as the change in area relative to its initial area, which was normalized to 100%. The resulting percentage values for each time point were then averaged for each experimental group and plotted. To ensure comparable results within a specific experimental setup, we evaluated the effect on spheroids that were selected based on their round morphology and similar initial size.

Viability of spheroids

To evaluate the cytotoxic effect of PAPBS on 3D tumor models, CellTiter-Glo® 3D Cell Viability Assay kit (Promega, Madison, Wisconsin, United States) was used. This assay measures cell viability based on the amount of adenosine triphosphate (ATP), which is directly proportional to the number of metabolically active cells. A luminescent signal is generated via an ATP-dependent luciferase reaction.

To measure viability, spheroids in 25 µl of DMEM were carefully transferred to white 96- well plate with clear flat bottom (SPL Life sciences). The CellTiter-Glo ® reagent was added in ratio 1:1. Plates were shaken for 20 min at room temperature, protected from light on orbital shaker. The luminescent signal was measured by using microplate reader The BioTek Synergy HTX [61].

Data analysis

Cell experiments were done in at least technical triplicates; spheroid experiments were done in at least sextuplicates. Three independent repeated experiments in each experimental condition were performed. The area of spheroids was measured from microscopic pictures using ImageJ software based on the scale in the pictures given by the microscope. Statistical averages and standard errors were calculated using Microsoft Excel. One-way ANOVA, which is a parametric test, was used to determine statistical significance of differences between the control group and the treated groups. All graphs and data visualizations were generated using OriginPro6.1.

Conclusion

This study successfully investigated and confirmed potential therapeutic efficacy of the PAPBS against breast cancer, even in cases of acquired drug resistance. PBS treated by cold atmospheric plasma generated by streamer corona discharge was characterized by a linear increase in RONS concentration relative to plasma activation time, with the concentration of RONS remaining stable for up to 24 h at 37°C. Plasma-activated PBS demonstrates significant and dose-dependent antitumor efficacy against 2D cell monolayers and 3D tumor models of human breast adenocarcinoma cells sensitive (MCF-7) or resistant (MCF-7/PAX) to paclitaxel. Notably, the drug-resistant spheroids demonstrated a higher susceptibility to PAPBS than the drug-sensitive spheroids. Resistant tumor models exposed 24 h to PAPBS treated 30 min by plasma completely lost their viability and structural integrity. These findings indicate that the PAPBS enriched by RONS generated by corona discharge represents a promising strategy against breast cancer especially in cases where tumors do not respond to currently available cytostatics.

Data availability

The datasets used and/or analysed during the current study is within the article and supplementary material. More experimental data is available from the corresponding author on reasonable request.

Received: 20 November 2025; Accepted: 23 February 2026

Published online: 05 March 2026

References

1. Bray, F. et al. Global cancer statistics 2022: GLOBOCAN estimates of incidence and mortality worldwide for 36 cancers in 185 countries. *CA. Cancer J. Clin.* **74**(3), 229–263. https://doi.org/10.3322/caac.21834 (2024).
2. Luqmani, Y. A. Mechanisms of drug resistance in cancer chemotherapy. *Med. Princ. Pract.* **14**(Suppl. 1), 35–48. https://doi.org/10.1159/000086183 (2005).
3. Fridman, G. et al. Applied plasma medicine. *Plasma Process. Polym.* **5**(6), 503–533. https://doi.org/10.1002/ppap.200700154 (2008).
4. Ono, R. Optical diagnostics of reactive species in atmospheric-pressure nonthermal plasma. *J. Phys. D Appl. Phys.* **49**(8), 083001. https://doi.org/10.1088/0022-3727/49/8/083001 (2016).
5. Graves, D. B. The emerging role of reactive oxygen and nitrogen species in redox biology and some implications for plasma applications to medicine and biology. *J. Phys. D Appl. Phys.* **45**(26), 263001. https://doi.org/10.1088/0022-3727/45/26/263001 (2012).
6. Lin, A. et al. Non-thermal plasma as a unique delivery system of short-lived reactive oxygen and nitrogen species for immunogenic cell death in melanoma cells. *Adv. Sci.* https://doi.org/10.1002/advs.201802062 (2019).
7. Furuta, R. et al. Intracellular responses to reactive oxygen and nitrogen species, and lipid peroxidation in apoptotic cells cultivated in plasma-activated medium. *Plasma Process. Polym.* **14**(11), 1700123. https://doi.org/10.1002/ppap.201700123 (2017).
8. Hirst, A. M. et al. Low-temperature plasma treatment induces DNA damage leading to necrotic cell death in primary prostate epithelial cells. *Br. J. Cancer* **112**(9), 1536–1545. https://doi.org/10.1038/bjc.2015.113 (2015).
9. Pelicano, H., Carney, D. & Huang, P. ROS stress in cancer cells and therapeutic implications. *Drug Resist. Updat.* **7**(2), 97–110. https://doi.org/10.1016/j.drup.2004.01.004 (2004).
10. Hecht, F. et al. Redox homeostasis of breast cancer lineages contributes to differential cell death response to exogenous hydrogen peroxide. *Life Sci.* **158**, 7–13. https://doi.org/10.1016/j.lfs.2016.06.016 (2016).
11. Jin, H.-O. et al. Piperlongumine induces cell death through ROS-mediated CHOP activation and potentiates TRAIL-induced cell death in breast cancer cells. *J. Cancer Res. Clin. Oncol.* **140**(12), 2039–2046. https://doi.org/10.1007/s00432-014-1777-1 (2014).
12. Chen, Y., McMillan-Ward, E., Kong, J., Israels, S. J. & Gibson, S. B. Oxidative stress induces autophagic cell death independent of apoptosis in transformed and cancer cells. *Cell Death Differ.* **15**(1), 171–182. https://doi.org/10.1038/sj.cdd.4402233 (2008).
13. Hileman, E. O., Liu, J., Albitar, M., Keating, M. J. & Huang, P. Intrinsic oxidative stress in cancer cells: A biochemical basis for therapeutic selectivity. *Cancer Chemother. Pharmacol.* **53**(3), 209–219. https://doi.org/10.1007/s00280-003-0726-5 (2004).
14. Babajani, A. et al. Reactive oxygen species from non-thermal gas plasma (CAP): Implication for targeting cancer stem cells. *Cancer Cell Int.* **24**(1), 344. https://doi.org/10.1186/s12935-024-03523-x (2024).
15. Szatrowski, T. P. & Nathan, C. F. Production of large amounts of hydrogen peroxide by human tumor cells. *Cancer Res.* **51**(3), 794–798 (1991).
16. Kong, Q., Beel, J. A. & Lillehei, K. O. A threshold concept for cancer therapy. *Med. Hypotheses.* **55**(1), 29–35. https://doi.org/10.1054/mehy.1999.0982 (2000).
17. Trachootham, D., Alexandre, J. & Huang, P. Targeting cancer cells by ROS-mediated mechanisms: A radical therapeutic approach?. *Nat. Rev. Drug Discov.* **8**(7), 579–591. https://doi.org/10.1038/nrd2803 (2009).
18. Verkman, A. S., Hara-Chikuma, M. & Papadopoulos, M. C. Aquaporins—new players in cancer biology. *J. Mol. Med.* **86**(5), 523–529. https://doi.org/10.1007/s00109-008-0303-9 (2008).
19. Kirkegaard, T., Riishede, A., Tramm, T. & Nejsum, L. N. Aquaglyceroporins in human breast cancer. *Cells* **12**(17), 2185. https://doi.org/10.3390/cells12172185 (2023).
20. Yusupov, M., Razzokov, J., Cordeiro, R. M. & Bogaerts, A. Transport of reactive oxygen and nitrogen species across aquaporin: A molecular level picture. *Oxid. Med. Cell Longev.* **2019**, 1–11. https://doi.org/10.1155/2019/2930504 (2019).
21. Van der Paal, J., Verheyen, C., Neyts, E. C. & Bogaerts, A. Hampering effect of cholesterol on the permeation of reactive oxygen species through phospholipids bilayer: Possible explanation for plasma cancer selectivity. *Sci. Rep.* **7**(1), 39526. https://doi.org/10.1038/srep39526 (2017).
22. Yan, D. et al. Toward understanding the selective anticancer capacity of cold atmospheric plasma—A model based on aquaporins (Review). *Biointerphases* https://doi.org/10.1116/1.4938020 (2015).
23. Bekeschus, S. et al. Tumor cell metabolism correlates with resistance to gas plasma treatment: The evaluation of three dogmas. *Free Radic. Biol. Med.* **167**, 12–28. https://doi.org/10.1016/j.freeradbiomed.2021.02.035 (2021).
24. Riethmüller, M., Burger, N. & Bauer, G. Singlet oxygen treatment of tumor cells triggers extracellular singlet oxygen generation, catalase inactivation and reactivation of intercellular apoptosis-inducing signaling. *Redox Biol.* **6**, 157–168. https://doi.org/10.1016/j.redox.2015.07.006 (2015).
25. Bauer, G. & Graves, D. B. Mechanisms of selective antitumor action of cold atmospheric plasma-derived reactive oxygen and nitrogen species. *Plasma Process. Polym.* **13**(12), 1157–1178. https://doi.org/10.1002/ppap.201600089 (2016).
26. Bauer, G., Sersenová, D., Graves, D. B. & Machala, Z. Dynamics of singlet oxygen-triggered, RONS-based apoptosis induction after treatment of tumor cells with cold atmospheric plasma or plasma-activated medium. *Sci. Rep.* **9**(1), 13931. https://doi.org/10.1038/s41598-019-50329-3 (2019).
27. Machala, Z. et al. Formation of ROS and RNS in water electro-sprayed through transient spark discharge in air and their bactericidal effects. *Plasma Process. Polym.* **10**(7), 649–659. https://doi.org/10.1002/ppap.201200113 (2013).
28. Lukes, P., Dolezalova, E., Sisrova, I. & Clupek, M. Aqueous-phase chemistry and bactericidal effects from an air discharge plasma in contact with water: Evidence for the formation of peroxynitrite through a pseudo-second-order post-discharge reaction of H_2O_2 and HNO_2. *Plasma Sources Sci. Technol.* **23**(1), 015019. https://doi.org/10.1088/0963-0252/23/1/015019 (2014).
29. Anderson, C. E., Cha, N. R., Lindsay, A. D., Clark, D. S. & Graves, D. B. The role of interfacial reactions in determining plasma–liquid chemistry. *Plasma Chem. Plasma Process.* **36**(6), 1393–1415. https://doi.org/10.1007/s11090-016-9742-1 (2016).
30. Gorbanev, Y., O'Connell, D. & Chechik, V. Non-thermal plasma in contact with water: The origin of species. *Chem. Eur. J.* **22**(10), 3496–3505. https://doi.org/10.1002/chem.201503771 (2016).
31. Takeda, S. et al. Intraperitoneal administration of plasma-activated medium: Proposal of a novel treatment option for peritoneal metastasis from gastric cancer. *Ann. Surg. Oncol.* **24**(5), 1188–1194. https://doi.org/10.1245/s10434-016-5759-1 (2017).
32. Adhikari, M. et al. Melanoma growth analysis in blood serum and tissue using xenograft model with response to cold atmospheric plasma activated medium. *Appl. Sci.* **9**(20), 4227. https://doi.org/10.3390/app9204227 (2019).
33. Sato, Y. et al. Effect of plasma-activated lactated Ringer's solution on pancreatic cancer cells in vitro and in vivo. *Ann. Surg. Oncol.* **25**(1), 299–307. https://doi.org/10.1245/s10434-017-6239-y (2018).
34. Nakamura, K. et al. Novel intraperitoneal treatment with non-thermal plasma-activated medium inhibits metastatic potential of ovarian cancer cells. *Sci. Rep.* **7**(1), 6085. https://doi.org/10.1038/s41598-017-05620-6 (2017).
35. Utsumi, F. et al. Effect of indirect nonequilibrium atmospheric pressure plasma on anti-proliferative activity against chronic chemo-resistant ovarian cancer cells in vitro and in vivo. *PLoS ONE* **8**(12), e81576. https://doi.org/10.1371/journal.pone.0081576 (2013).
36. Mihai, C.-T. et al. Cold atmospheric plasma-activated media improve paclitaxel efficacy on breast cancer cells in a combined treatment model. *Curr. Issues Mol. Biol.* **44**(5), 1995–2014. https://doi.org/10.3390/cimb44050135 (2022).

37. Yan, D. et al. Stabilizing the cold plasma-stimulated medium by regulating medium's composition. *Sci. Rep.* **6**(1), 26016. https://doi.org/10.1038/srep26016 (2016).
38. Biscop, E. et al. The influence of cell type and culture medium on determining cancer selectivity of cold atmospheric plasma treatment. *Cancers (Basel)* **11**(9), 1287. https://doi.org/10.3390/cancers11091287 (2019).
39. Veronico, V. et al. Anticancer effects of plasma-treated water solutions from clinically approved infusion liquids supplemented with organic molecules. *ACS Omega* **8**(37), 33723–33736. https://doi.org/10.1021/acsomega.3c04061 (2023).
40. Zhang, J. et al. Investigation of different solutions activated by air plasma jet and their anticancer effect. *Appl. Phys. Lett.* https://doi.org/10.1063/5.0096605 (2022).
41. Lee, S. et al. Cold atmospheric plasma restores tamoxifen sensitivity in resistant MCF-7 breast cancer cell. *Free Radic. Biol. Med.* **110**, 280–290. https://doi.org/10.1016/j.freeradbiomed.2017.06.017 (2017).
42. Park, S. et al. Cold atmospheric plasma restores paclitaxel sensitivity to paclitaxel-resistant breast cancer cells by reversing expression of resistance-related genes. *Cancers (Basel)* **11**(12), 2011. https://doi.org/10.3390/cancers11122011 (2019).
43. Jordan, M. A. et al. Mitotic block induced in HeLa cells by low concentrations of paclitaxel (Taxol) results in abnormal mitotic exit and apoptotic cell death. *Cancer Res.* **56**(4), 816–825 (1996).
44. Alexandre, J., Hu, Y., Lu, W., Pelicano, H. & Huang, P. Novel action of paclitaxel against cancer cells: Bystander effect mediated by reactive oxygen species. *Cancer Res.* **67**(8), 3512–3517. https://doi.org/10.1158/0008-5472.CAN-06-3914 (2007).
45. Jelínek, M. et al. Substituents at the C3′ and C3′N positions are critical for taxanes to overcome acquired resistance of cancer cells to paclitaxel. *Toxicol. Appl. Pharmacol.* **347**, 79–91. https://doi.org/10.1016/j.taap.2018.04.002 (2018).
46. Němcová-Fürstová, V. et al. Characterization of acquired paclitaxel resistance of breast cancer cells and involvement of ABC transporters. *Toxicol. Appl. Pharmacol.* **310**, 215–228. https://doi.org/10.1016/j.taap.2016.09.020 (2016).
47. Pampaloni, F., Reynaud, E. G. & Stelzer, E. H. K. The third dimension bridges the gap between cell culture and live tissue. *Nat Rev Mol Cell Biol* **8**(10), 839–845. https://doi.org/10.1038/nrm2236 (2007).
48. Machala, Z., Tarabová, B., Sersenová, D., Janda, M. & Hensel, K. Chemical and antibacterial effects of plasma activated water: correlation with gaseous and aqueous reactive oxygen and nitrogen species, plasma sources and air flow conditions. *J Phys D Appl Phys* **52**(3), 034002. https://doi.org/10.1088/1361-6463/aae807 (2019).
49. Sersenová, D., Machala, Z., Repiská, V. & Gbelcová, H. Selective Apoptotic Effect of Plasma Activated Liquids on Human Cancer Cell Lines. *Molecules* **26**(14), 4254. https://doi.org/10.3390/molecules26144254 (2021).
50. Van Boxem, W. et al. Anti-cancer capacity of plasma-treated PBS: effect of chemical composition on cancer cell cytotoxicity. *Sci Rep* **7**(1), 16478. https://doi.org/10.1038/s41598-017-16758-8 (2017).
51. Aggelopoulos, C. A. et al. Cold atmospheric plasma attenuates breast cancer cell growth through regulation of cell microenvironment effectors. *Front. Oncol.* https://doi.org/10.3389/fonc.2021.826865 (2022).
52. Qi, M. et al. In vivo metabolic analysis of the anticancer effects of plasma-activated saline in three tumor animal Models. *Biomedicines* **10**(3), 528. https://doi.org/10.3390/biomedicines10030528 (2022).
53. Griseti, E., Merbahi, N. & Golzio, M. Anti-cancer potential of two plasma-activated liquids: implication of long-lived reactive oxygen and nitrogen species. *Cancers (Basel)* **12**(3), 721. https://doi.org/10.3390/cancers12030721 (2020).
54. Girard, P.-M. et al. Synergistic effect of H2O2 and NO2 in cell death induced by cold atmospheric He plasma. *Sci Rep* **6**(1), 29098. https://doi.org/10.1038/srep29098 (2016).
55. Griseti, E. et al. Pulsed electric field treatment enhances the cytotoxicity of plasma-activated liquids in a three-dimensional human colorectal cancer cell model. *Sci. Rep.* https://doi.org/10.1038/s41598-019-44087-5 (2019).
56. Bekeschus, S. et al. Cold physical plasma-treated buffered saline solution as effective agent against pancreatic cancer cells. *Anticancer Agents Med Chem* **18**(6), 824–831. https://doi.org/10.2174/1871520618666180507130243 (2018).
57. Yi, P. N. et al. Swelling of multicellular spheroids induced by hyperthermia. *Int. J. Hyperth.* **3**(3), 217–233. https://doi.org/10.3109/02656738709140389 (1987).
58. Kerr, J. F. R., Wyllie, A. H. & Currie, A. R. Apoptosis: a basic biological phenomenon with wideranging implications in tissue kinetics. *Br J Cancer* **26**(4), 239–257. https://doi.org/10.1038/bjc.1972.33 (1972).
59. Majno, G. & Joris, I. Apoptosis, oncosis, and necrosis. An overview of cell death. *Am. J. Pathol.* **146**(1), 3–15 (1995).
60. Eisenberg, G. Colorimetric determination of hydrogen peroxide. *Ind. Eng. Chem. Anal. Ed.* **15**(5), 327–328. https://doi.org/10.1021/i560117a011 (1943).
61. Riss, T. et al. Validation of in vitro assays to measure cytotoxicity in 3D cell cultures. *Toxicol Lett* **229**, S145. https://doi.org/10.1016/j.toxlet.2014.06.508 (2014).

Author contributions

D.K. ran and processed the experiments and wrote the initial draft of the manuscript. H.G. supervised the experiments with cells and spheroids, reviewed and edited the manuscript. Z.M. conceptualized and supervised the research, reviewed, and edited the manuscript. All authors have provided partial funding, and read and agreed to the published version of the manuscript.

Funding

This work was supported by Slovak Research and Development Agency, grants APVV-22-0247 and APVV-17-0382 and Comenius University grants UK/3193/2024 and UK/1369/2025; with a support of EU NextGenerationEU through the Recovery and Resilience Plan for Slovakia under the projects No. 09I03-03-V05-00012 and 09I03-03-V03-00033.

Declarations

Competing interests

The authors declare no competing interests.

Additional information

Supplementary Information The online version contains supplementary material available at https://doi.org/10.1038/s41598-026-41704-y.

Correspondence and requests for materials should be addressed to Z.M.

Reprints and permissions information is available at www.nature.com/reprints.

Publisher's note Springer Nature remains neutral with regard to jurisdictional claims in published maps and institutional affiliations.

Open Access This article is licensed under a Creative Commons Attribution-NonCommercial-NoDerivatives 4.0 International License, which permits any non-commercial use, sharing, distribution and reproduction in any medium or format, as long as you give appropriate credit to the original author(s) and the source, provide a link to the Creative Commons licence, and indicate if you modified the licensed material. You do not have permission under this licence to share adapted material derived from this article or parts of it. The images or other third party material in this article are included in the article's Creative Commons licence, unless indicated otherwise in a credit line to the material. If material is not included in the article's Creative Commons licence and your intended use is not permitted by statutory regulation or exceeds the permitted use, you will need to obtain permission directly from the copyright holder. To view a copy of this licence, visit http://creativecommons.org/licenses/by-nc-nd/4.0/.

© The Author(s) 2026